4-1999

The I-Band Tully-Fisher Relation for Sc Galaxies: Optical Imaging Data

Martha P. Haynes
Center for Radiophysics and Space Research and National Astronomy and Ionosphere Center

Riccardo Giovanelli
Center for Radiophysics and Space Research and National Astronomy and Ionosphere Center

John J. Salzer
Wesleyan University

Gary Wegner
Dartmouth College

THE ASTRONOMICAL JOURNAL, 117:1668–1687, 1999 April

THE *I*-BAND TULLY-FISHER RELATION FOR Sc GALAXIES: OPTICAL IMAGING DATA

MARTHA P. HAYNES AND RICCARDO GIOVANELLI
Center for Radiophysics and Space Research and National Astronomy and Ionosphere Center,[1] Cornell University, Ithaca, NY 14853; haynes@astrosun.tn.cornell.edu, riccardo@astrosun.tn.cornell.edu

JOHN J. SALZER
Department of Astronomy, Wesleyan University, Middletown, CT 06459; slaz@parcha.astro.wesleyan.edu

GARY WEGNER
Department of Physics and Astronomy, Dartmouth College, Hanover, NH 03755; wegner@kayz.dartmouth.edu

WOLFRAM FREUDLING
Space Telescope European Coordinating Facility and European Southern Observatory, Karl-Schwarzschild-Strasse 2, D-85748 Garching bei München, Germany; wfreudli@eso.org

LUIZ N. DA COSTA
European Southern Observatory, Karl-Schwarzschild-Strasse 2, D-85748 Garching bei München, Germany; ldacosta@eso.org

TERRY HERTER
Center for Radiophysics and Space Research, Cornell University, Ithaca, NY 14853; herter@astrosun.tn.cornell.edu

AND

NICOLE P. VOGT
Institute of Astronomy, University of Cambridge, Madingley Road, Cambridge CB3 0HA, UK; nicole@ast.cam.ac.uk
Received 1998 November 2; accepted 1998 December 28

ABSTRACT

Properties derived from the analysis of photometric *I*-band imaging observations are presented for 1727 inclined spiral galaxies, mostly of types Sbc and Sc. The reduction, parameter extraction, and error estimation procedures are discussed in detail. The asymptotic behavior of the magnitude curve of growth and the radial variation in ellipticity and position angle are used in combination with the linearity of the surface brightness falloff to fit the disk portion of the profile. Total *I*-band magnitudes are calculated by extrapolating the detected surface brightness profile to a radius of eight disk scale lengths. Errors in the magnitudes, typically ~ 0.04 mag, are dominated by uncertainties in the sky subtraction and disk-fitting procedures. Comparison is made with the similar imaging database of Mathewson, Ford, & Buchhorn, both as presented originally by those authors and after reanalyzing their digital reduction files using identical disk-fitting procedures. Direct comparison is made of profile details for 292 galaxies observed in common. Although some differences occur, good agreement is found, proving that the two data sets can be used in combination with only minor accommodation of those differences. The compilation of optical properties presented here is optimized for use in applications of the Tully-Fisher relation as a secondary distance indicator in studies of the local peculiar velocity field.

Key words: galaxies: photometry — galaxies: spiral — techniques: photometric

1. INTRODUCTION

In a series of papers, this group has employed the *I*-band Tully-Fisher (TF) relation to derive aspects of the local peculiar velocity field (da Costa et al. 1996, 1998; Giovanelli et al. 1996, 1997a, 1998a, 1998c, 1998d; Borgani et al. 1997; Freudling et al. 1998). The observational ingredients required for these studies include an estimate of the rotation velocity width derived from either 21 cm H I line profiles (Haynes et al. 1997, 1998) or optical emission-line rotation curves (Giovanelli et al. 1997b, 1998b) and ellipticities and total magnitudes derived from optical images. We have also used the observational data set to explore the effects of internal extinction in galaxies (Giovanelli et al. 1994, hereafter G94) and its dependence on galaxy luminosity (Giovanelli et al. 1995, hereafter G95). In this paper we discuss in detail the optical imaging observations and their associated reduction procedures and present the compilation of relevant galactic properties.

The observational sample presented here is a mixture of targets selected as good TF candidates from three main categories: (1) spiral galaxies in nearby clusters, the SCI sample (Giovanelli et al. 1997b, 1997c); (2) field Sc galaxies, the SFI sample (G94; G95; Freudling et al. 1995; Wegner et al. 1998); and (3) selected other spirals, particularly in the region of the Pisces-Perseus supercluster. Because different catalogs were used to make up the initial target list and the imaging program had multiple goals, the final imaging sample presented here is rather heterogeneous. The present compilation, referred to as the Sc sample, consists primarily of Sbc–Sc spirals but includes all objects imaged with high quality in the *I* band, some of which do not fit the final criteria of the SFI or SCI samples.

Simultaneously with the current study, Mathewson, Ford, & Buchhorn (1992) and Mathewson & Ford (1996, hereafter MF96) conducted a similar *I*-band survey of mainly Sc galaxies, mostly in the southern hemisphere, also for the purpose of applying the *I*-band TF relation. In addition to the final compilation of parameters adopted for TF use, Mathewson & Ford have made available the digital data files containing the results of their isophotal analysis of the imaging data. We refer to this combined data set, both

[1] The National Astronomy and Ionosphere Center is operated by Cornell University under a cooperative agreement with the National Science Foundation.

TABLE 1

SUMMARY OF INSTRUMENT PARAMETERS BY OBSERVING PERIOD

Telescope	Detector	Format	Scale (arcsec pixel^{-1})	Gain (e^- ADU^{-1})	Read Noise (e^-)	Date	Number of Galaxies
CTIO 0.9 m	Tek 4	512 × 512	0.445	3.13	7.0	1990 Oct	29
	Thomson	512 × 512	0.64	3.23	4.0	1990 Oct	28
	Thomson No. 2	512 × 512	0.626	1.91	3.4	1991 Mar	153
	Tek1K-1	1024 × 1024	0.396	3.10	5.3	1992 Apr	50
KPNO 0.9 m.....	Tek 1	512 × 512	0.77	10.05	8.0	1988 Oct	142
	Tek 1	512 × 512	0.77	3.25	7.8	1990 May	1[a]
	ST1K	1024 × 1024	0.60	2.7	3.0	1991 Apr	64
	TE1K	1024 × 1024	0.68	3.2	4.0	1991 Apr	82
	T2KA	1024 × 1024	0.68	2.6	3.6	1992 Mar	128
	T2KA	1024 × 1024	0.68	10.5	4.0	1992 Oct	41
MDM 1.3 m	RCA	512 × 320	0.625	17.48	64.0	1988 Oct	275
						1989 Apr	132
						1989 Jun	191
						1989 Oct	44
						1989 Dec	23
						1990 Mar	104
						1990 Sep	6
						1990 Oct	307
						1990 Nov	30
						1991 Jan	92
						1991 Mar	58
						1991 Oct	73
	Loral (Wilbur)	1024 × 1024[b]	0.635	1.94	6.0	1992 Dec	26

[a] Image observed as part of survey of Freudling et al. 1991.
[b] CCD is 2048 × 2048; 2 × 2 binning option employed.

the tabulation as presented by MF96 and the digital data files, as the MFB set. An early understanding of the two groups was that the samples could eventually be combined to produce a final database with all-sky coverage. We are now able to conduct the comparison of the two data sets to explore the possibility of using them in combination.

This paper presents the details of the *I*-band optical imaging component of our TF survey data. In § 2 we describe the procedures associated with image acquisition and reduction. Section 3 presents the results of the image reduction for 1727 objects and reviews the characteristics of the imaging data. A comparison of the current survey with that of the MFB set, including a direct cross-check of 292 galaxies imaged by both groups, is presented in § 4. The main conclusions are summarized in § 5.

2. DETAILS OF IMAGING OBSERVATIONS AND REDUCTION PROCEDURES

Optical *I*-band photometric imaging observations were conducted over a 5 yr period from 1988 October to 1992 October with the 1.3 m McGraw-Hill telescope of the Michigan-Dartmouth-MIT Observatory (MDM),[2] the 0.9 m telescope of the Kitt Peak National Observatory (KPNO),[3] and the 0.9 m telescope of the Cerro Tololo Inter-American Observatory (CTIO).[4] Nearly all exposures were of 600 s duration and were obtained under photometric conditions. Typical sky backgrounds of 300–600 counts were detected in 600 s, yielding rms noise levels of order 1%–2% of the sky level (5.5–6.9 counts for the RCA CCD on the MDM 1.3 m, for example).

A listing of observing runs along with the relevant telescope and detector information is given in Table 1, along with the number of analyzed images obtained in each observing period. The tabulated information for each telescope and detector includes the CCD format, pixel scale, gain, and read noise, as well as the number of images obtained in each observing period that were analyzed. Sixty-five percent of the images were obtained at MDM, 22% at KPNO, and 13% at CTIO. One image, that of UGC 8356, was taken from the survey of Freudling, Martel, & Haynes (1991). A total of 2079 images of 1830 galaxies were analyzed; several hundred additional frames of poor quality were discarded at the outset. A final sample containing 1727 galaxies was constructed after averaging multiple frames of galaxies observed more than once and discarding frames that were of low quality or that were deemed inappropriate for TF studies (poor flat-fielding, stellar contamination, galaxy interactions, etc.). Throughout the process we have attempted to keep the data collection and reduction procedure as uniform as possible.

The flat-fielding and photometric reduction for all runs except the two-cluster subsample ones (1991 April and 1992 March) were performed by J. J. S. The same tasks for the two cluster subsamples were undertaken by T. H. and N. V.

[2] The MDM Observatory was operated jointly by the University of Michigan, Dartmouth College, and the Massachusetts Institute of Technology on Kitt Peak, Arizona, during the time these observations were made.

[3] The Kitt Peak National Observatory is part of the National Optical Astronomy Observatories (NOAO), operated by Associated Universities for Research in Astronomy (AURA), Inc., under a cooperative agreement with the National Science Foundation (NSF).

[4] The Cerro Tololo Inter-American Observatory is part of the NOAO, operated by AURA, Inc., under a cooperative agreement with the NSF.

Images were debiased, trimmed, and flat-fielded using standard IRAF[5] procedures. Flat fields have been obtained by constructing a median flat from object frames observed over one or more nights within a single observing run. For the smaller CCDs, care was taken to move the target galaxies around the CCD so that a good flat could be obtained from the combination of object frames. Typically, 30–50 object frames were used in the construction of the median flat.

Our images in the I band suffered from fringing to varying degrees, depending on the CCD used. However, since for all runs we created flat-field images from the galaxy images, we automatically had a suitable fringe correction image as well. We found that, in most cases, the fringe pattern was completely removed from our fully processed images and hence fringing was not a major limitation to the accuracy of our isophote fitting or galaxy photometry.

Since each observing run was characterized by a different set of photometric calibrations, uniformity of the calibration procedure has been of paramount importance. Photometric calibration was achieved by nightly observations of standard stars chosen from the list of Landolt (1983). Typically eight to 25 standard star observations were interspersed with the program galaxies on each night that data were acquired. Extinction coefficients and zero-point constants were obtained nightly, and color coefficients (in $R-I$) were determined at least once and sometimes twice per run. Although no color information was available for our sample of galaxies (we imaged only in the I band), we observed standards in the R and I bands to determine the color coefficients, assumed a mean galaxy $R-I$ color of 0.50 ± 0.10 (Freudling 1990), and included the color term in the magnitude equation. All measurements and photometric analyses of the standard stars were carried out by J. J. S., with the exception of the two cluster subsample runs mentioned above. Typical formal uncertainties in the I-band nightly zero-point constants were 0.005–0.020 mag. Of the nights with usable data, 92% had uncertainties in the zero-point constant of less than 0.025 mag. Galaxies observed on nights with lower quality photometry were often reobserved during subsequent runs.

Further reduction of the images was performed within the IRAF/STSDAS[6] environment using a set of scripts developed initially by W. F. and J. J. S. and further modified and extended by M. P. H. and J. J. S., referred to hereafter as the GALPHOT package. A constant value associated with the sky background was subtracted using an iterative procedure that allows the user to mark boxes on the frame that are free of bright stars and galaxies. The adopted sky value is the mean intensity obtained from each "sky" box, after automatically masking the faint stars and galaxies within the box. Sky boxes were positioned far enough from the galaxy (at least two galaxy radii as estimated by eye on the image but typically not much more than that) to ensure that the background level was not affected by the light from the outer parts of the galaxy, but close enough that the sky level measured was appropriate for the galaxy. Overall, the degree of flatness of the images was high; coupled with the "local" nature of the background measurement of the sky brightness, the adoption of the mean sky level measured in the various sky boxes (as opposed to a higher order surface fit) was adequate. Typically, four to six sky boxes were employed, and the scatter among the individual values was characteristically 0.1%–0.2% of the background level (or less).

Cosmic rays and stars have been masked by a two-step process. First, a rectangular box of twice the dimension of, and centered on, the galaxy was outlined interactively. Outside this box, masking was performed automatically; within it, stars and cosmic rays were masked interactively. Within the galaxy itself, care was taken to identify superposed stars but not to mask H II regions. Sky subtraction and masking was performed by G. W., M. P. H., J. J. S., L. N. dC., T. H., and N. V. for different subsets.

In the interest of consistency, reduction of all images from the final masking stage to completion was performed by M. P. H. Elliptical surface brightness contours were fitted using a modified version of the STSDAS package ISOPHOTE. The primary modifications made to ISOPHOTE were (1) to "dampen" the fit, i.e., for a given isophote, the parameters of the fit from iteration to iteration were allowed to vary more slowly than in the original code by adding only a fraction of the computed correction. This modification was necessary for early versions of ISOPHOTE, which, as coded, did not work well on spiral galaxies (Freudling 1990); and (2) the inclusion of an option to halt the outward iterations when the mean intensity of the computed isophote is less than the rms noise level.

An initial starting guess for the ellipse-fitting routine was provided by interactively marking points that represent the ends of the major and minor axes at an isophotal level of relatively high signal-to-noise ratio. The ellipse centroid, position angle, and ellipticity were allowed to vary slightly from successive ellipses. In many cases, multiple fits were obtained, varying the initial guess in order to obtain a "best" fit. A display of the contours superposed on the image, as well as the variations with the semimajor axis of the ellipse centroid, position angle, ellipticity, total magnitude, surface magnitude, rms, number of data points, and number of interactions, was examined in deciding on the best fit. The output of ISOPHOTE was kept in instrumental units, for calibration at a later stage.

The disk portion of the surface brightness profile was then fitted using an interactive procedure that allows specification of the inner and outer disk radii, as discussed by G94. On "marking the disk," a linear function was fitted to the surface brightness profile over the portion of the profile identified as the disk and the slope and intercept of this fit were recorded. The inverse of the slope is proportional to the observed disk scale length. Also recorded were the mean position angle of the disk, its mean ellipticity, and centroid X and Y pixel values and their errors. Note that the ellipticity is defined as $\epsilon = 1 - b/a$, where a and b are the major and minor axis diameters, respectively.

Because the isophote-fitting process tends to increase artificially the axial ratio (b/a) for highly inclined galaxies or ones with large bulges, the mean isophotal ellipticity values underestimate the true flatness for such galaxies. As a first step to counteract this effect, a maximum ellipticity was also recorded, taken to be the maximum of a running average of the ellipticity values measured at sequential isophotes in the

[5] IRAF (Image Reduction and Analysis Facility) is distributed by NOAO, which is operated by AURA under a cooperative agreement with the NSF.

[6] STSDAS (Space Telescope Science Data Analysis System) is distributed by Space Telescope Science Institute, which is operated by AURA under contract to the National Aeronautics and Space Administration.

outer portion of the disk. The number of isophotes used in calculating this running average was adjusted according to the size of the galaxy and ranged from five to nine. In general, the maximum and mean ellipticities agreed within their calculated errors and differed significantly only when the galaxy was highly inclined ($\epsilon > 0.8$) and/or contained a significant bulge. In those cases the maximum value clearly provided a better estimate and thus was adopted. For the most extreme edge-on cases, the light profiles at several cuts perpendicular to the disk were examined to determine the appropriate value to record. In all cases, the images were inspected to decide what value of the ellipticity (mean, maximum, or interactively measured) to adopt. A correction for seeing was then applied, following G94. For these images, the median seeing was 1.″5–1.″6. The adopted error on the ellipticity is the error on the mean or maximum value, as appropriate.

Disk fitting even late spiral galaxies is notoriously fraught with uncertainty. Knapen & van der Kruit (1991) have discussed the wide variation in disk scale lengths found for the same galaxy by different authors. For example, because of extinction, the surface brightness profiles of inclined galaxies tend to steepen toward the outer edge, so that scale lengths measured in the inner disk will be larger than those measured further out. Here disks were fitted interactively for two distinct purposes: (1) to extract mean properties of the disk such as ellipticity and position angle and to explore the effects of internal extinction (G94; G95) and (2) to extrapolate the light profile beyond the detected edge to obtain a total magnitude. Because the presence of structure (bars, spiral arms, etc.) and the effects of extinction affect the disk fit, the best fits for the two purposes are not necessarily the same; this point is also discussed by Willick (1999). The largest variations occur in highly inclined systems for which the profile shows a steep drop at the outermost radii or in systems for which a single exponential does not match the disk well, for example, Freeman type II profiles (Freeman 1970; de Jong 1996). As part of the analysis presented by G94 and G95, we have experimented with different fitting techniques, using both automatic and interactive procedures. For the current purposes, a more sophisticated bulge-disk decomposition scheme was not deemed to be necessary. The fit adopted for the extrapolation typically begins at a surface magnitude fainter than 22 mag arcsec^{-2} and extends to the second to last measured radial point along the major axis. The final adopted parameters reflect the best fit in both a quantitative and qualitative sense.

The ellipse fitting was used to construct a model of the galaxy that itself was then used for interpolation over the masked regions. Magnitudes were then calculated using the IRAF routine POLYPHOT to measure the total flux within the ellipses. A variety of magnitudes was recorded by interpolation or extrapolation of ones computed at each isophote, both magnitudes at fixed isophotal levels and partial magnitudes integrated to a certain number of disk scale lengths.

As discussed by G94 and G95, isophotal magnitudes are influenced by extinction effects; a total magnitude, calculated by analytically extrapolating the disk fit beyond the outermost isophote to infinity, was obtained. However, because a radial truncation in the stellar disks of edge-on spirals is commonly observed (e.g., van der Kruit 1979; van der Kruit & Searle 1981) and because the sky background dominates the uncertainty, we elect to adopt in this work a total magnitude m_I computed at a radius of eight disk scale lengths $8r_d$. Because of the uncertainty in the outermost detected isophotes, the extrapolation is begun at least one isophote inward of the last, after the disk is fitted. Note that this truncated m_I is about 0.01–0.02 mag fainter than the magnitude extrapolated to infinity. The median amplitude of the extrapolation from the outermost measured isophote included in the disk fit to $8r_d$ is 0.05 mag. Surface brightnesses were measured out to a median isophotal level of 23.97 mag arcsec^{-2}, or $\sim 4.2r_d$.

Errors in the computed magnitudes at each isophote arise from a number of sources; we account for five distinct contributions:

1. Poisson errors due to the total flux in each aperture.
2. Poisson noise from the sky flux, associated with each pixel. Although a mean sky background is subtracted in accounting for the sky, each pixel has associated with it a $\sqrt{N}$ uncertainty due to the sky contribution. Over the image, this error can be fairly treated as a constant uncertainty per pixel, but it has to be multiplied by the square root of the number of pixels in each elliptical aperture.
3. The uncertainty in the determination of the sky level. Formally, this is the rms noise in the portions selected to represent the sky (taken as the standard deviation of the pixel distribution in the sky boxes, after masking the stars contained within them), scaled by the number of pixels in each aperture used to measure the galactic light. In the end, errors in the total magnitudes are probably dominated by the uncertainty (not the formal uncertainty) in the background removal, especially for large apertures. Typically, this uncertainty is on the order of 0.1%–0.2% of the background level. In reality, this error should also account for imperfect flat-fielding; however, there is no good way to estimate this uncertainty for any given image. We estimate the contribution to the error for the uncertainty in the sky determination to be equal to 15% of the total sky standard deviation.
4. Error in the photometric calibration for each night. Because we retained only high-quality photometric data from the start, errors in the photometric zero-point calibration were always less than 0.05 mag and typically better than 0.02 mag.
5. Errors in the magnitudes arising from differences in the intrinsic galaxy color. The computation of our I-band magnitudes includes a color term of the form $\epsilon(R-I)$, where ϵ is the color coefficient derived from observations of standard stars and $R-I$ is the color the galaxy. In general, we do not have color information for our galaxy sample, hence $R-I$ is unknown. We adopt a mean value of $R-I = 0.50 \pm 0.1$ (Freudling 1990) based on the mean color of Sbc-Sc galaxies included in Pierce & Tully (1988). Although the colors of spiral galaxies certainly do show some spread, the coefficient of the color term is small ($\langle\epsilon\rangle \sim 0.04$), so that errors in the adopted color are negligible in comparison with others.

Other types of errors such as flat-field errors, the contributions of stars in the galaxy apertures, scattered light, and so on also enter in but are impossible to estimate. We believe that our derived errors are conservative and also reflect the relative quality of individual values.

Since total magnitudes are computed by extrapolation beyond the detected disk, we include an estimate of the error in the extrapolation process as an additional com-

ponent equal to $0.2\delta m$, where $\delta m = m_{\rm edge} - m_I$. This term is added in quadrature to the error determined for the optical edge using the five terms listed above. Typical total errors σ_m lie in the range 0.03–0.06 mag, with a median value of 0.044.

For 108 galaxies, more than one high-quality image was obtained in separate observing sessions, mostly with different telescopes/instrument configurations. In constructing the final parameters, results derived from individual frames were averaged, weighting each according to its photometric accuracy and discarding images of lower quality. Comparison of the magnitudes obtained separately shows consistency within the estimated errors, and no systematic differences among the observing sessions were detected.

Isophotal radii are also calculated and recorded, at surface brightness levels between 22 and 24.5 mag arcsec^{-2} in steps of 0.5 mag arcsec^{-2}. As discussed by G94, the measured isophotal diameter is affected by internal extinction and thus depends on inclination. Because we desire to define a characteristic radius for the purposes of adopting a uniform measure of rotational velocity (Giovanelli et al. 1998b), an "optical radius," r_{83L}, is determined as that radius within which is found 83% of the total galaxy luminosity (Persic, Salucci, & Stel 1996). Note that r_{83L} is defined such that $m(r_{83L}) = m_I + 0.2023$.

To demonstrate the fitting and extrapolation process, Figure 1 shows results for the edge-on SBc galaxy AGC 27566 = ESO 569-G14 observed with the CTIO 0.9 m telescope in 1991 March. Derived properties for this galaxy are listed in Table 5. The left-hand panels show the results of the analysis of the Sc image, and the right-hand panels display a similar analysis performed on the comparable digital tabulation from the MFB set, as discussed in § 4. From top to bottom are displayed, respectively, the variations along the major axis, at each fit ellipse, of the total magnitude, $m_I(r)$; the position angle, $\theta(r)$; the ellipticity, $\epsilon(r)$;

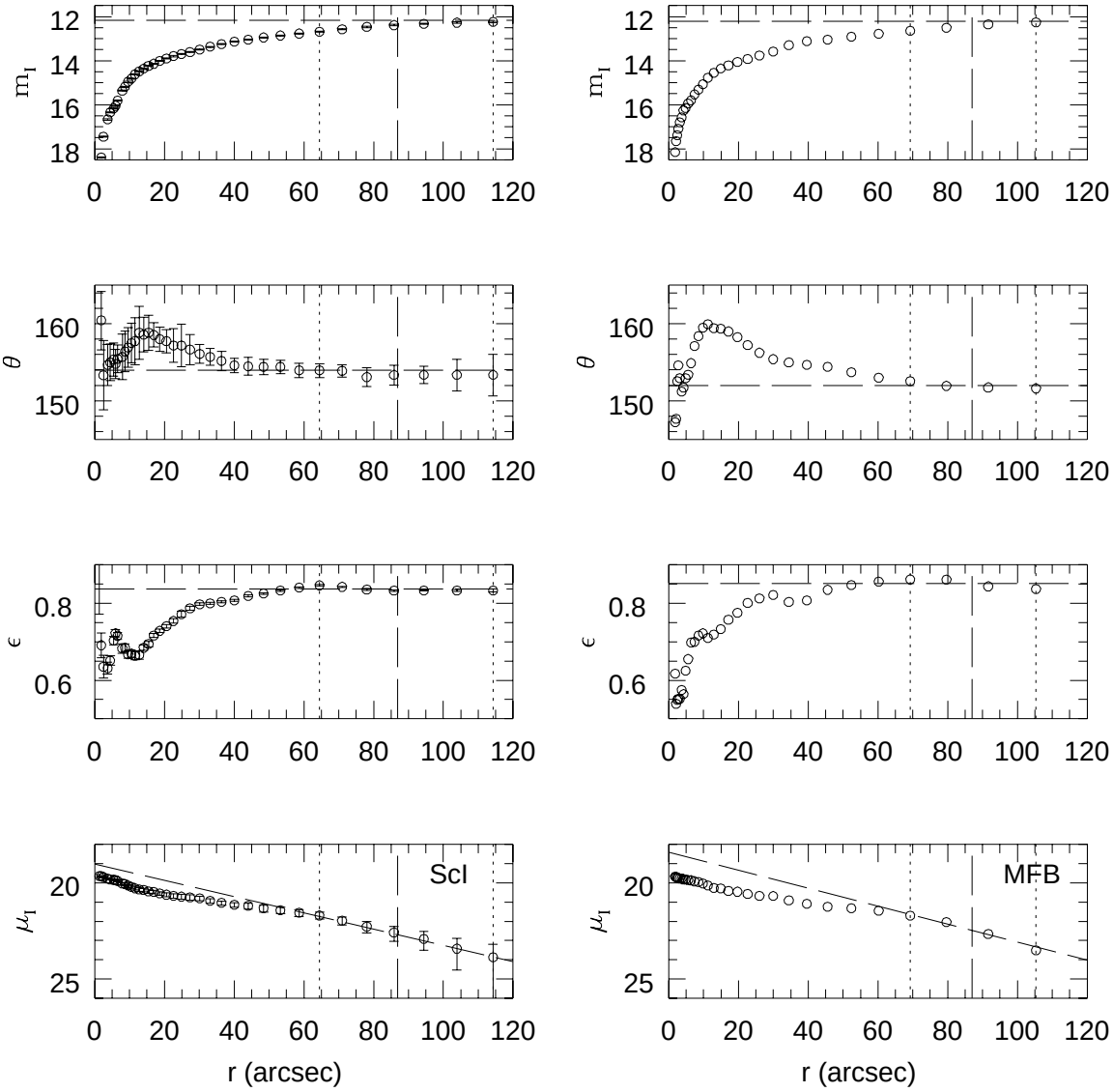

FIG. 1.—Example of the disk-fitting and extrapolation procedure for the edge-on galaxy AGC 27566 = ESO 569-G14 based on GALPHOT processing of the Sc I-band image (*left*) and the MFB digital ellipse-fit tabulation (*right*). Panels display, from top to bottom, the variation with increasing distance along the major axis of the results of the ellipse-fitting procedure for total magnitude $m_I(r)$, position angle $\theta(r)$, ellipticity $\epsilon(r)$, and surface magnitude $\mu(r)$. Error bars are indicated for the Sc analysis. In the top three panels, the horizontal dashed line indicates the final adopted parameter for the disk (m_I, θ, and ϵ_0). In each panel, dotted vertical lines denote the portion of the profile used for fitting the disk, and the dashed vertical line marks the characteristic optical radius r_{83L}. In the bottom panel, the disk fit used in the extrapolation of the magnitude is displayed.

and the surface magnitude, $\mu(r)$. In each panel, the inner and outer radii selected when "marking the disk" are indicated by dotted vertical lines. A dashed vertical line marks the characteristic optical radius, r_{83L}. Dashed horizontal lines mark the final adopted values of m_I, θ, and ϵ_0 in the top three panels, respectively. The sloped dashed line in the bottom panel shows the disk fit used to extrapolate the profile beyond the last detected isophote to obtain m_I at $8r_d$. For this galaxy $\mu_{\rm edge} = 23.80$ and $\delta m = 0.049$. The comparison with the MFB analysis is discussed in § 4. The cataloged major and minor diameters are 5.0 and 0.8, respectively, or $1 - (b/a) = 0.84$; analysis of the I-band images produces equivalent measures of the ellipticity $\epsilon = 0.837$ for both the average and maximum methods, corrected for a seeing FWHM of 2.0, $\epsilon_0 = 0.843$. This image is illustrative of several points concerning the fitting process. Because this galaxy is viewed edge-on, the surface brightness profile steepens at surface magnitudes fainter than about 21.5 mag arcsec^{-2} where the disk becomes transparent. A single exponential cannot be fitted to both the inner and outer disks. It is clear from the fit used to extrapolate the magnitude that the disk central surface brightness, μ_0, is overestimated. A more reasonable value would be obtained if the profile were fitted inward of that portion used here; however, in that case, the extrapolation to $8r_d$ would result in an underestimate of the magnitude, making the galaxy too bright. For the purpose of extrapolating the profile to derive the total magnitude, the fit should be restricted, as evident in Figure 1, to the outer portion where the profile begins to steepen. At the same radius that the profile drops, the ellipticity and position angle also approach their constant outer values. It is the combination of this asymptotic behavior and profile steepening that dictates our choice of disk fit. Otherwise, a scale length measured in the inner disk would differ by as much as 30% from that given by the outer disk fit, resulting in an overestimate of the magnitude by 0.19 mag. It is important to note therefore that in highly inclined systems, profiles must extend deep enough to detect this change of slope (van der Kruit 1979). In this study we preferentially fitted the outer portions of disks, at isophotes fainter than 22 mag arcsec^{-2}. Further discussion of this comparison is included in the Appendix.

In the Appendix we present additional examples of representative data to illustrate the range of galaxy profiles and discuss specific cases demonstrating the uncertainties that arise in the disk-fitting process. It is important to note that the dominant errors in the magnitude arise not from the photometric calibration but rather from uncertainty in the sky subtraction and disk-fitting procedure.

3. DATA PRESENTATION

The properties of the galaxies in the optical Sc sample are presented individually in Table 2, which is available in its entirety only electronically. Entries in the table are as follows:

Column (*1*).—Entry number in the Uppsala General Catalog (UGC) (Nilson 1973), where applicable, or else in our private database, referred to as the Arecibo General Catalog (AGC).

Column (*2*).—NGC or IC designation, or other name, typically from the Catalog of Galaxies and of Clusters of Galaxies (CGCG) (Zwicky et al. 1960), the ESO-Uppsala Catalog (ESO) (Lauberts 1982), or the Morphological Catalog of Galaxies (MCG) (Vorontsov-Velyaminov & Arhipova 1968).

Columns (*3*) *and* (*4*).—Right ascension and declination in the 1950.0 epoch, either from the literature or measured by us on the POSS-I. Typically, the listed positions have 15″ accuracy.

Column (*5*).—The morphological type code, T, following the RC3 (de Vaucouleurs et al. 1991) system. Classification comes either from the UGC or ESO catalogs, the RC3, the Southern Equatorial Galaxy Catalog (H. G. Corwin 1982, private communication), or from our own visual examination of the POSS-I prints. A "B" indicates the presence of a bar.

Column (*6*).—The isophotal radius measured at an I-band surface magnitude of 23.5 mag arcsec^2, $r_{23.5}$, in arcseconds.

Column (*7*).—The characteristic optical radius, r_{83L}, in arcseconds, derived from the image and corresponding to that radius encompassing 83% of the total galactic light.

Column (*8*).—The surface magnitude at the other most detected isophote in the I-band image, $\mu_{\rm edge}$, in mag arcsec^2.

Column (*9*).—The disk ellipticity, ϵ_0, corrected for seeing following G94, and its associated error, σ_ϵ.

Column (*10*).—The mean disk position angle, θ, and its associated error, σ_θ, in degrees. It should be noted, as evident in Figure 3, that the ellipse-fitting procedure is not able to constrain θ well for low-inclination objects, $\epsilon_0 < 0.4$.

Column (*11*).—The total I-band magnitude, m_I, extrapolated to $8r_d$, and its associated error σ_m.

In Table 3 and Figure 2 we summarize the characteristic properties of the Sc imaging data. Listed in Table 3 are the average and median values and the standard deviation of the distribution of the following properties of the 1727 gal-

TABLE 2

OPTICAL PROPERTIES

AGC Number (1)	NGC/IC (2)	α (1950) (3)	δ (1950) (4)	T (5)	$r_{23.5}$ (arcsec) (6)	r_{83L} (arcsec) (7)	$\mu_{\rm out}$ (8)	eps$_0$ (9)	θ (deg) (10)	m_I (11)
400001	MCG −10-10-24	000001.0	−035920	4B	31.6	23.2	23.83	0.450 ± 0.094	180 ± 4	12.90 ± 0.02
14	478-019	000101.2	+225519	5	55.5	49.2	23.93	0.408 ± 0.056	27 ± 8	12.33 ± 0.07
19	N7817	000124.8	+202818	4	106.1	67.6	23.95	0.736 ± 0.024	47 ± 4	10.65 ± 0.02
24	478-020	000139.5	+221840	5B	28.7	37.6	23.12	0.462 ± 0.096	46 ± 14	13.98 ± 0.07
25	MCG +10-10-20	000151.5	+055353	5	28.1	21.0	23.83	0.746 ± 0.032	126 ± 2	14.17 ± 0.03

NOTE.—Table 2 is presented in its entirety in the electronic edition of the Astronomical Journal. A portion is shown here for guidance regarding its form and content.

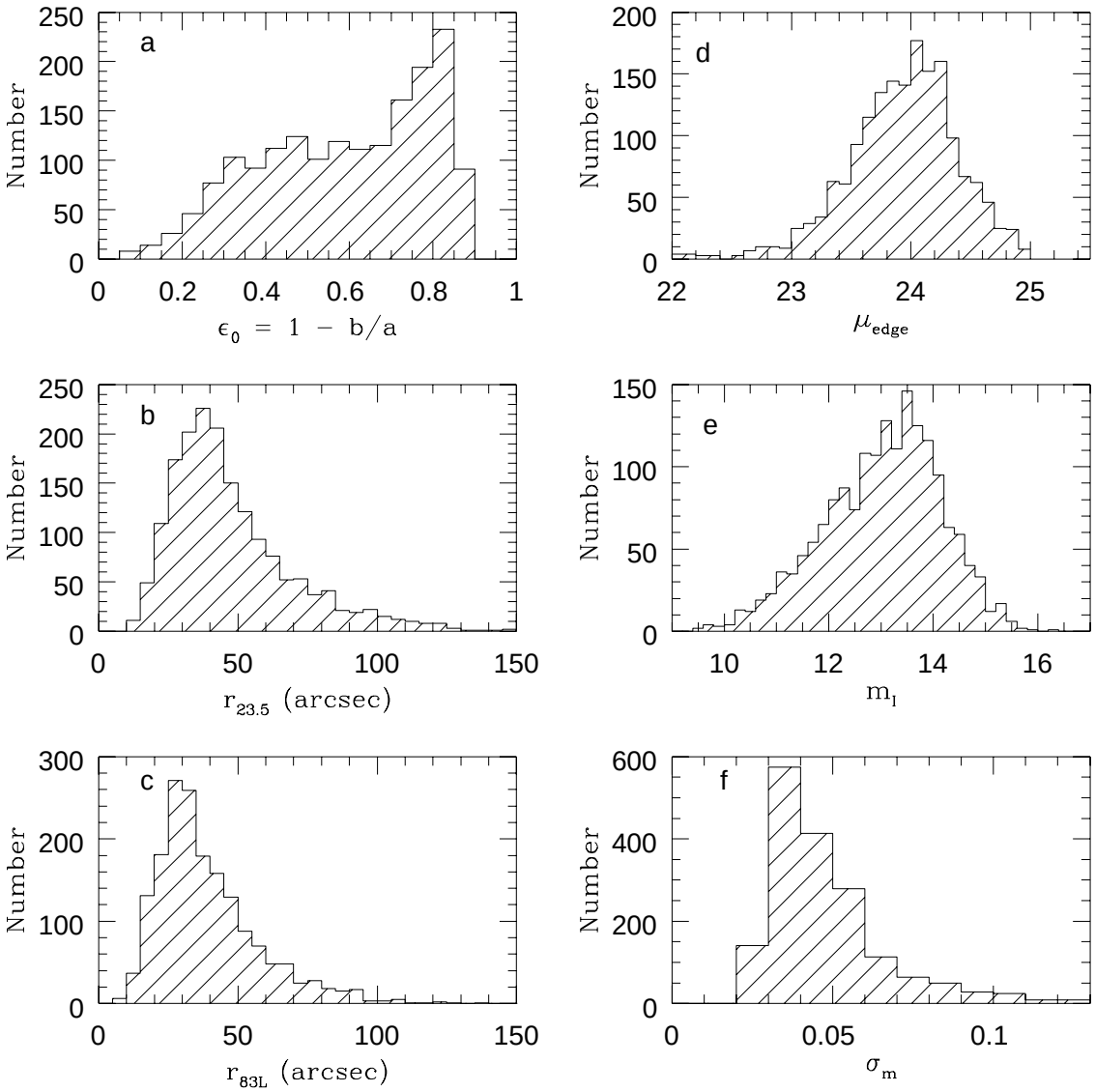

FIG. 2.—Characteristics of Sc imaging results. Panels *a–e* show, respectively, histograms of the distributions of ϵ_0, $r_{23.5}$, r_{83L}, μ_{edge}, m_I, and σ_m.

axies in the Sc sample: ϵ_0, $r_{23.5}$, r_{83L}, the surface magnitude at the radius where the extrapolation is begun μ_{r2}, μ_{edge}, m_I, and σ_m. Figure 2 shows histograms of the distributions of all but μ_{r2}. A few relevant points should be noted: (1) The sample, designed for application of the TF relation, includes few low-inclination galaxies and a corresponding overrepresentation by high-inclination objects. (2) The sample is not magnitude limited in any sense. (3) The *I*-band images are deep enough to extend beyond r_{83L} and to include portions where the surface brightness profile steepens. (4) Typical errors in the derived total magnitudes are $\sim$0.04 but are sometimes twice as large; uncertainties in the photometric zero point are typically less than 0.02 mag.

In Figure 3 we compare derived values of $r_{23.5}$, θ, and ϵ_0 with corresponding ones available from the UGC and ESO compilations. Panels *a* and *b* show the comparison between the catalog major axis radii and the measured values of $r_{23.5}$. Because of the differences in scaling of the UGC and the ESO catalog (e.g., Paturel et al. 1991), comparisons are shown separately for each. Plotted in each panel is a line of slope 1 (*solid line*) and the least-squares fit ($y = a + bx$). Note that the cataloged diameters are quantized at the 0.1 level. The correspondence is clear, although the scatter is large. In the *I* band, $r_{23.5}$ is about 20% smaller than the cataloged radii; further discussion on this subject was presented by G94.

Panel *c* of Figure 3 shows the variation in the difference in the derived position angle θ with that contained in the UGC and the ESO catalog as a function of ϵ_0. Errors in position angle are usually small, of order 2°–3°, except at low inclinations $\epsilon_0 < 0.4$. The ellipse-fitting routine is not able to constrain well the position angles for face-on galaxies, especially when spiral structure is strong. Panel *d* shows the variation of the ellipticity derived from cataloged diameters with the image values of ϵ_0. The line of slope 1 is superposed; note that the cataloged values of the diameters are quantized so that some quantization in $1 - (b/a)$ is seen. There is some tendency at the highest ellipticities for the cataloged values to be greater than the derived ones; in fact, the cataloged values sometimes suggest axial ratios that are unrealistically too flat, given an intrinsic axial ratio for Sc galaxies of $q = 0.13$ (G94).

In the next section, we discuss the comparison of the Sc data set with the previously published results of MFB,

TABLE 3

COMPARISON OF ANALYSIS OF Sc AND MFB SAMPLES

PARAMETER	Sc			MFB		
	Average	Standard Deviation	Median	Average	Standard Deviation	Median
Total Sample ($N_{Sc}=1727$, $N_{MFB}=2370$)						
ϵ_0	0.59	0.20	0.63	0.58	0.18	0.59
$r_{23.5}$ (arcsec)	47.7	22.8	41.7	49.0	30.6	41.5
r_{83L} (arcsec)	39.2	18.9	34.5	39.9	25.6	33.4
μ_{r2} (mag arcsec^{-2})	23.27	0.47	23.30	23.20	0.65	23.21
μ_{edge} (mag arcsec^{-2})	23.94	0.48	23.97	24.24	0.58[a]	24.26
m_I	13.03	0.90	13.14	13.00	1.19	13.10
σ_m	0.04	0.02	0.04	0.04	0.01[b]	0.04
Overlap Sample ($N_{Sc}=N_{MFB}=292$)						
ϵ_0	0.60	0.19	0.64	0.60	0.19	0.64
$r_{23.5}$ (arcsec)	58.5	23.9	52.7	58.8	23.2	52.2
r_{83L} (arcsec)	46.3	17.6	43.1	46.1	16.7	43.6
μ_{r2} (mag arcsec^{-2})	23.28	0.46	23.36	23.20	0.63	23.23
μ_{edge} (mag arcsec^{-2})	23.91	0.43	23.96	24.25	0.53[a]	24.24
m_I	12.55	1.10	12.49	12.55	1.07	12.55
σ_m	0.04	0.02	0.04	0.04	0.01[b]	0.04

[a] The outermost isophotes of the MFB profiles have not been truncated at low noise in the same manner as done for the Sc data set.

[b] The standard deviation for the MFB sample is likely to be underestimated because the error information is derived from a simplified algorithm, not actual values.

demonstrating the efficacy of using the two in combination to derive the local peculiar velocity field.

4. COMPARISON WITH THE MFB SAMPLE

MFB presented results for their *I*-band photometric survey of 2447 mainly southern spirals, also conducted for the purpose of determination of the local peculiar velocity field by application of the TF relation. In order to establish coordination of our mutual efforts, R. G. and M. P. H. spent 6 weeks at the Mount Stromlo and Siding Springs Observatory during the early phases of both programs, participating in brief observing sessions for both radio spectroscopy at Parkes and optical imaging at Siding Springs. Although the remainder of the observations, data analysis, and reduction was carried out independently, some collaborative understanding was exchanged. Of current relevance is that about 300 galaxies were imaged by both groups.

MF96 present a tabular summary of their derived parameters for 2447 galaxies. Their method of calculating magnitudes and ellipticities is somewhat different from that employed here. Because use of different methods to extract properties may introduce systematic (and subtle) differences in the derived parameters that might not be treated by developing recursion relations and because other relevant parameters were not included in that tabulation, we have made use of data files provided by D. Mathewson and V. Ford containing the results of their ellipse-fitting procedure. The original tables were converted to a format compatible for processing within GALPHOT and reexamined using the procedures described in § 2 to fit disks and derive mean ellipticities and total magnitudes and their associated errors in an attempt to derive a homogeneous combined data set. By this process we have elected to discard some of the MFB data where uncertainty in the identification of the galaxy or the data quality arises. We derive relevant parameters for 2370 of the 2447 galaxies presented in MF96.

Not all of the detailed information, particularly that on errors, available for our images is contained in the MFB imaging data files. We estimate comparable errors as follows: For the position angle, we estimate the errors according to the surface brightness and the typical variation in the errors found in the Sc isophotal profiles. In the inner portions of the disk [$\mu(r) < 19$ mag arcsec^{-1}], errors on the total magnitude, ellipticity, position angle, and surface magnitude were assumed to be 0.02, 0.04, 3°.0, and 0.02, respectively. Further out, the errors in magnitude and surface magnitude varied with surface magnitude and the errors in ellipticity and position angle were correlated with the ellipticity, being larger for face-on galaxies. The adopted values are conservative and, in fact, probably underestimate the true errors. Because of the use of these recipes rather than true errors, the distribution of the estimated errors of these properties shows an artificially smaller spread than for the Sc data.

On occasion, the MFB profiles extend beyond $\mu(r) > 25$ mag arcsec^{-1}. We believe that, in many cases, this extension is artificial, resulting from a lack of termination of the ellipse-fitting algorithm at low noise. Where the surface magnitude flattens (or even rises) beyond $\mu(r) > 25$ mag arcsec^{-1} in the MFB data, we truncate the profiles at this level. Additionally there is a sign/orientation ambiguity in the MFB position angles that generates false values of average position angle and its error so that we do not compare the derived values with those found in our own analysis. A uniform seeing disk of FWHM = 1.″2 was adopted.

Table 3 and Figure 4 summarize the results for the 2370 MFB galaxies that we have reanalyzed. Figures 2 and 4 are directly comparable. The Sc and MFB samples are quite similar in many respects, although there are a few notable differences. The MFB sample contains larger populations of low-inclination objects and low surface brightness ones; as

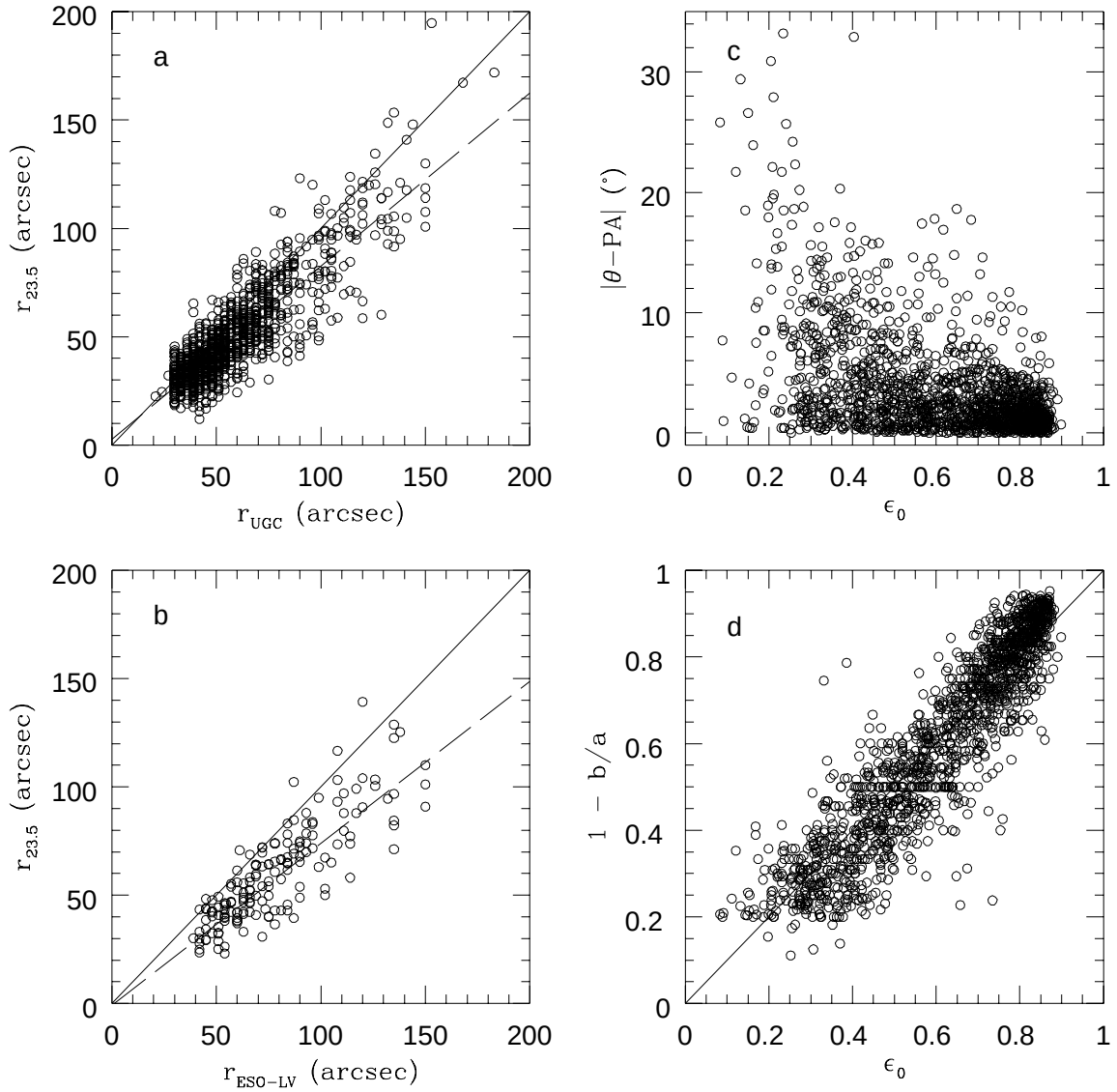

FIG. 3.—Comparison of derived position angles and ellipticities with estimates from cataloged parameters

discussed by Wegner et al. (1998), the SFI sample was specifically designed to maintain constant low surface brightness limits at all redshifts. Although the MFB profiles appear to extend deeper, this result is likely to arise from the stricter truncation criterion in fitting the outer isophotes adopted in analyzing the Sc images; typical values of the outermost significant points used in the disk-fitting procedure occur at quite similar levels (μ_{r2}). The MF96 compilation gives inclinations, not ellipticities, derived under the assumption that the intrinsic axial ratio is 0.20, so that $\epsilon \leq 0.8$. The observed ellipticities, however, are sometimes flatter than this, giving rise to larger values of ϵ than are recoverable from the MF96 tabulation.

It should be noted that the total magnitude given in MF96 is defined as that contained within an elliptical aperture out to 25 mag arcsec^{-2}, corresponding roughly to $\sim 5r_d$, whereas the analysis performed here extrapolates the magnitude to $8r_d$. We expect, therefore, a systematic difference in the magnitude scales between our method and that of MF96 at a level of about 0.03–0.04 mag, with our magnitudes being systematically brighter by that amount.

For 292 galaxies, isophotal analysis results are available from both MFB and the Sc images; furthermore, some of the properties (e.g., m_i, ϵ_0, $r_{23.5}$) extracted from the isophotal analysis can be directly compared with ones listed in the MF96 data compilation. Table 3 also includes the summary of the common subsets. In fact, the comparison is excellent. Whereas this agreement may not be surprising given that the galaxies are the same, it nonetheless provides reassurance that the analysis procedures produce consistent results.

Table 4 and Figure 5 illustrate the comparison of the three common data sets for the 292 galaxies: (1) the Sc imaging data, (2) our reanalysis of the MFB data files (MFB_{fit}), and (3) the MF96 data compilation. Figure 5 shows the variation in magnitude differences $m_i - m_j$ among the three data sets as a function of magnitude in one of them in panels *a*–*c*. Panel *d* shows the variation in $m_i - m_j$ with $a_{23.5}$ as derived for the Sc images. The expected systematic relative brightness of the magnitudes extrapolated to $8r_d$ is not seen; the effect is only half as great. As evident in Figures 5*b* and 5*d*, there is some tendency for the

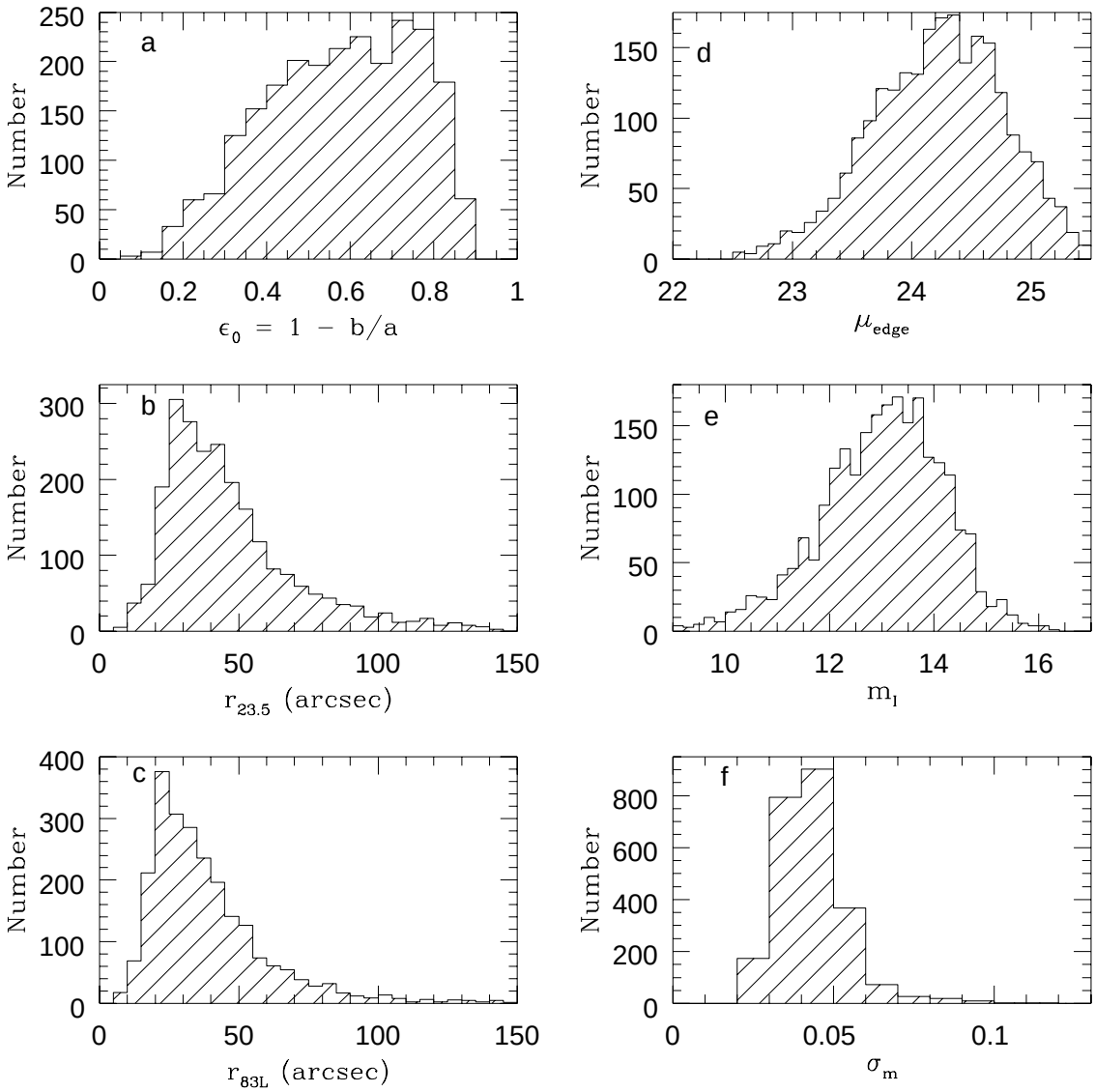

FIG. 4.—Characteristics of reanalysis of MFB results. Similar to Fig. 2, panels *a*–*e* show the histograms of the distributions of ϵ_0, $r_{23.5}$, r_{83L}, μ_{edge}, m_I, and σ_m.

Sc magnitudes to vary systematically from the ones presented in MF96, both at the bright and faint (also large and small) ends. On average, the discrepancies are minor, but the reprocessing of the MFB profiles through GALPHOT helps to decrease this trend (decreasing the regression slope from 0.034 to 0.031); reprocessing also allowed us to eliminate the most discrepant cases (e.g., where the images did not extend deep enough). We suspect that this trend arises for reasons associated with the depth of the images (at the faint end) and the sky subtraction (at the bright end), but the exact causes remain unclear. The smaller scatter in Figure 5*c* is not surprising since photometric errors and/or systematic differences should not play a role.

Of the 292 objects in common, 161 were observed by us at CTIO, 115 at MDM, and 16 at KPNO. No systematic differences are present in the comparison of the MDM and CTIO subsets with the MFB data sets; the KPNO one is too small to be statistically significant.

TABLE 4

COMPARISON OF RESULTS FOR 292 GALAXIES IN Sc AND MFB

	1 VERSUS 2			1 VERSUS 3			2 VERSUS 3		
PARAMETER	Average	Standard Deviation	Median	Average	Standard Deviation	Median	Average	Standard Deviation	Median
$m_I(i)$-$m_I(j)$	−0.001	0.11	−0.01	0.017	0.13	0.00	0.018	0.07	0.01
$r_{23.5}(i)/r_{23.5}(j)$.....	0.99	0.07	1.00	1.00	0.08	1.01	1.01	0.04	1.01
$\epsilon(i)/\epsilon(j)$	1.01	0.13	0.99	1.04	0.15	1.01	1.03	0.08	1.02

NOTE.—Samples $i, j = 1, 2, 3$ refer to (1) the Sc imaging data, (2) the reanalysis of the MFB ellipse output tables, and (3) the tabulation in MF96, respectively.

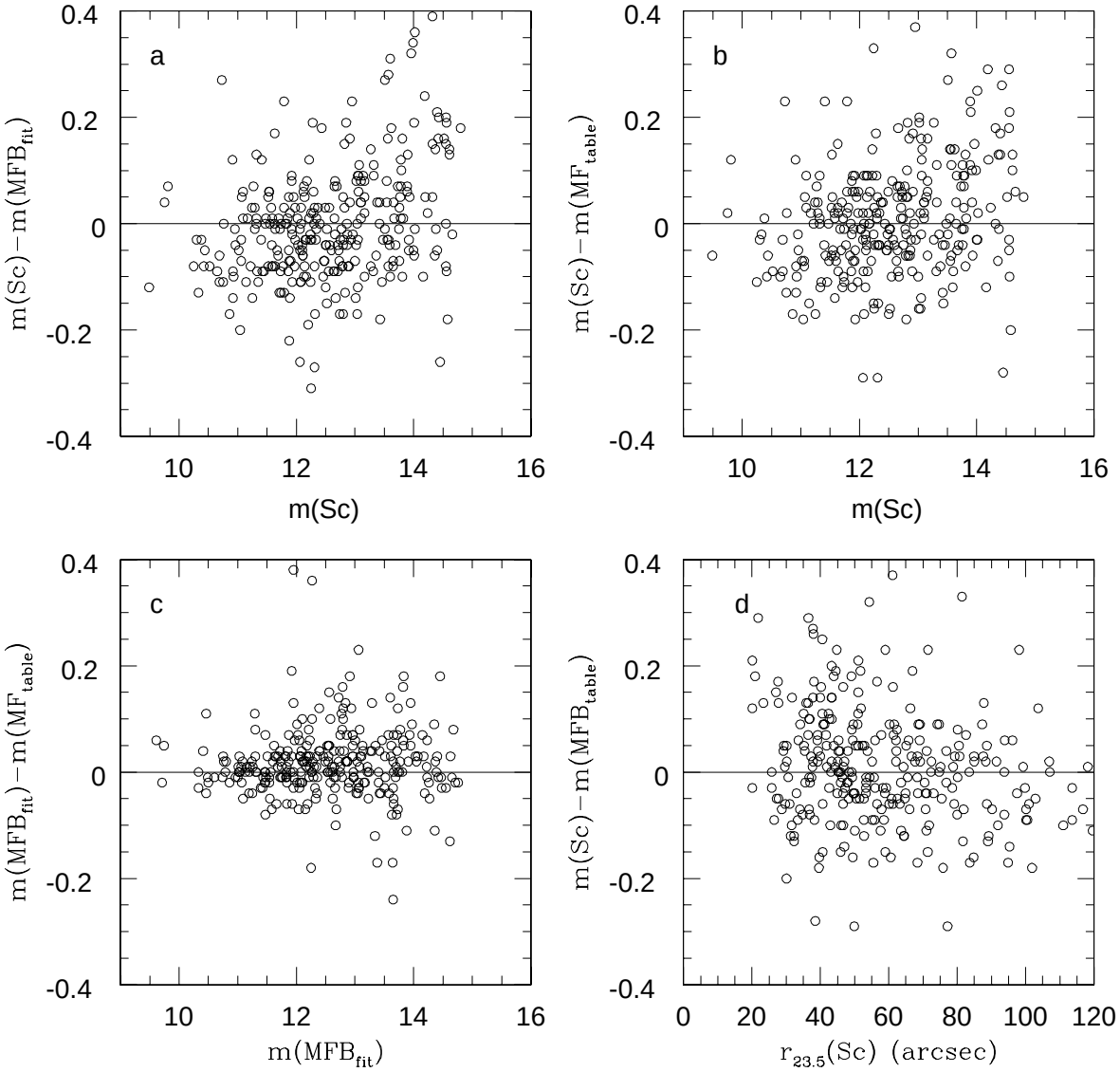

FIG. 5.—Comparison of the derived magnitudes of the Sc sample and the MFB sample both as reprocessed by us (MFB_{fit}) and contained in tabular form in MF96 (MF_{table}).

Besides providing additional parameters not available in the MF96 compilation, the reanalysis of the MFB data files also produces somewhat more consistency between the Sc and MFB. Overall, we find remarkably good agreement, confirming that the two data sets can be used in combination.

5. SUMMARY

The *I*-band imaging survey presented here derives isophotal and characteristic radii, disk ellipticities, and total magnitudes for 1727 galaxies, primarily inclined, late-type spirals. The main points can be summarized as follows:

1. The objective of the imaging survey has been to produce parameters to be used in the application of the TF relation, namely total magnitudes and inclinations and their associated errors. The galaxies whose properties are presented here include all objects for which high-quality images were obtained and analyzed, including some that are not included in the analyses presented elsewhere, i.e., the SFI and SCI samples.

2. Total magnitudes, m_I, are derived by extrapolating from the outermost edge to a radius corresponding to $8r_d$. Truncation at that radius is performed rather than extrapolating to infinity because optical edges are seen in deep studies of highly inclined spirals. The extrapolation beyond the faintest detected isophote follows the disk marked interactively for that purpose.

3. Typical errors in the derived magnitudes are $\sim$0.04 mag but are sometimes twice as large. Uncertainties in the photometric zero point are nearly always less than 0.02 mag. The estimated error includes a term associated with the extrapolation to $8r_d$. The error is dominated by uncertainties in the determination of the sky contribution.

4. The ellipticity of the disk, ϵ_0, is derived either from an average over the disk portion or from the maximum of a running average across the disk. In most cases, the two agree within the errors. For highly inclined galaxies or ones of more moderate inclination with large bulges, the ellipse-fitting procedure underestimates the ellipticity. In such cases, ϵ_0 is estimated from the visual inspection of vertical cuts perpendicular to the disk. The ellipticity is not well

constrained for face-on objects, which are, in any event, underrepresented in this TF sample.

5. In addition to the isophotal radius, $r_{23.5}$, a characteristic radius, r_{83L}, is derived, corresponding to that radius containing 83% of the total light. The images are typically deep enough to extend beyond r_{83L}.

6. The errors in position angle are typically small, of order 2°–3°. However, at low inclination ($\epsilon_0 < 0.4$) the position angle is not well constrained.

7. A comparison of 292 galaxies contained both in the current data set and in the compilation of MFB reveals generally good agreement of derived parameters, within their estimated errors.

These imaging data, in combination with velocity widths derived from optical or radio H I line spectra, provide the main ingredients for the TF studies undertaken by this group. Combination with the results presented by MFB, shown here to be comparable in quality (as deliberately planned), allows investigation of the local velocity field from an all-sky sample.

This research has been partially supported by NSF grants AST90-14850, AST92-18038, and AST95-28860 to M. P. H. and T. H.; AST90-23450 to M. P. H.; AST91-15459, AST94-20505, and AST96-17069 to R. G.; AST95-53020 to J. J. S.; and AST93-47714 to G. W. G. W. wishes to thank the Cornell University Department of Astronomy for hospitality and partial support for his sabbatical visit in 1992. R. G. and M. P. H. acknowledge the support of fellowships from the Australian National University and the hospitality of the Mount Stromlo and Siding Springs Observatory for their visit at the earliest stages of this project, and they thank Vince Ford and Don Mathewson for providing a digital version of their data set. This work has made use of the NASA/IPAC Extragalactic Database, which is operated by the Jet Propulsion Laboratory, California Institute of Technology, under contract with the National Aeronautics and Space Administration. We very much appreciate the excellent assistance provided by the staffs at the various observatories, particularly Bob Barr at MDM.

APPENDIX A

EXAMPLES OF DISK-FITTING AND EXTRAPOLATION PROCEDURE

The error in the derived magnitude is a combination of the photometric accuracy, the uncertainty in determination of the sky level, and the extrapolation of the disk fit. The latter depends on the intrinsic shape of the light profile and the galaxy inclination. Figures 1 and 6–12 demonstrate a variety of cases of disk fitting and a graphic comparison of the fitting procedures for both the Sc images and the MFB ellipse fit data files. Each display is identical to that described for Figure 1 in § 2. The profiles are indeed similar (as expected; it is the same galaxy, after all!). Note that because errors in most properties are not included in the MFB data files, errors have been estimated by means of algorithmic prescriptions. Errors bars are thus not shown for the MFB fit. Table 5 lists the values of $r_{23.5}$, ϵ_0, and m_I for the three available data sets: Sc images, the reanalysis of the MFB profiles (MFB_{fit}), and the MF96 compilation. Note that these are representative but not average profiles; these have been chosen specifically to demonstrate certain points, particularly discrepancies. Here we discuss each case separately.

AGC 27566 = ESO 569-G14.—Figure 1 was discussed in part in § 2. The figure also shows the comparable fit to the MFB profile data set, displayed similarly. The Sc analysis appears to show better convergence of the ellipse parameters toward the outer parts. As evident in Table 5, the derived properties for this galaxy are very similar in the three data sets. Because Mathewson & Ford adopt an intrinsic axial ratio of 0.2 for disks, conversion of their tabulated inclination to an ellipticity produces a maximum value of 0.8, although both sets of ellipses indicate that the object is somewhat flatter.

AGC 450071 = MCG −2-15-006.—Figure 6 examines the case of MCG −2-15-006, a highly inclined, flattened disk, much smaller in size than ESO 569-G14 (Fig. 1). The MFB data sets give brighter values of m_I by about 0.1 mag, possibly because of uncertain contributions fainter than $\mu > 24$ mag arcsec^{-2}. As in the case of ESO 569-G14, we adopt the maximum ellipticity rather than the average; as before, the Sc value is larger than either of the MFB ones.

TABLE 5

I-BAND PROPERTIES OF GALAXIES CITED AS EXAMPLES

		Sc			MFB_{fit}			MF96		
AGC	NAME	$r_{23.5}$ (arcsec)	ϵ_0	m_I	$r_{23.5}$ (arcsec)	ϵ_0	m_I	$r_{23.5}$ (arcsec)	ϵ	m_I
27566	569-G14	107.1	0.843 ± 0.005	12.17 ± 0.04	108.8	0.854 ± 0.012	12.20 ± 0.04	105.0	0.800	12.17
450071.....	MCG −21-50-06	36.7	0.857 ± 0.006	14.61 ± 0.03	32.9	0.836 ± 0.013	14.50 ± 0.05	36.6	0.800	14.51
430121.....	MCG −20-90-21	40.0	0.830 ± 0.014	14.24 ± 0.04	38.7	0.809 ± 0.026	14.22 ± 0.04	38.4	0.783	14.21
139.....	382-035	45.9	0.598 ± 0.036	12.93 ± 0.05	45.5	0.577 ± 0.041	12.96 ± 0.04	45.0	0.540	12.93
400367.....	MCG −10-30-05	46.7	0.718 ± 0.007	13.46 ± 0.04	43.6	0.719 ± 0.027	13.57 ±0.04	43.2	0.715	13.50
260112.....	108-108	20.1	0.307 ± 0.049	14.00 ± 0.04	19.1	0.272 ± 0.084	14.05 ± 0.04	19.2	0.279	14.03
630027.....	MCG −25-90-01	20.1	0.488 ± 0.036	14.56 ± 0.04	20.2	0.356 ± 0.159	14.37 ± 0.05	17.4	0.256	14.35
31271	515-G5	21.8	0.539 ± 0.032	14.19 ± 0.07	26.8	0.579 ± 0.048	13.95 ± 0.05	39.6	0.610	13.90

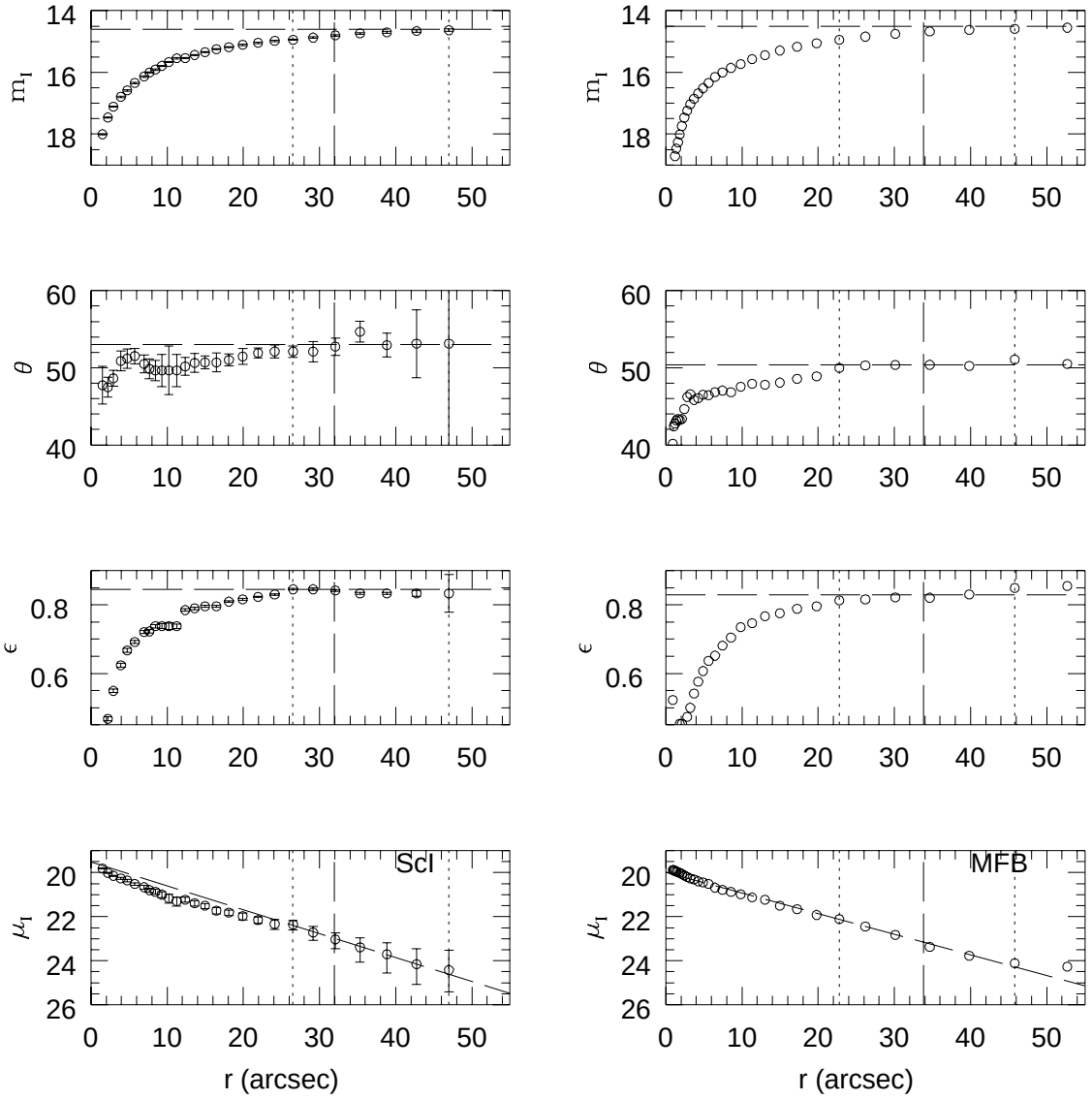

FIG. 6.—Comparison of fitting procedures and results for AGC 400571 = MCG −2-15-006. Panels and indicated lines are the same as in Fig. 1.

AGC 430121 = MCG −2-09-021.—Figure 7 compares the fits for MCG −2-09-021, a highly inclined spiral with evidence of dust and a prominent spiral arm on its southwestern side. The central portion of the profile is very shallow, with no evidence of a bulge. A change of slope is clearly evident at $\mu(r) \sim 22$ mag arcsec^{-2} in both profiles. The three values of m_I agree, but the MF96 compilation adopts a smaller inclination as evident in Table 5.

UGC 139 = CGCG 382-035.—Figure 8 shows the results for UGC 139, a moderate-inclination Sc galaxy. Evidence of the spiral structure is seen in the smooth variations in $\epsilon(r)$ and $\theta(r)$ and the corresponding wiggles in the surface magnitude profile $\mu(r)$. Examination of the image dictated the adoption of the maximum disk ellipticity rather than the average in deriving ϵ_0 for the Sc data set, resulting in a somewhat larger value than estimated by MF96. The three data sets give consistent values of $r_{23.5}$ and m_I.

AGC 400367 = MCG −1-03-005.—Figure 9 shows the comparison of the Sc and MFB analysis for MCG −1-03-005, a moderate-inclination Sc galaxy with a patchy disk. Detection of the change of slope in the profile at faint isophotes, evident in both profiles, is critical in the extrapolation of the magnitude. For comparison, we also fitted beginning at $r = 17''.8$ ($\mu = 21.50$ mag arcsec^{-2}) yielding a total magnitude $m_I = 13.40$, rather than 13.46 for the Sc image, and a lower ellipticity by about 0.02.

AGC 260112 = CGCG 108-108.—Figure 10 displays the comparison for CGCG 108−108, a small, distant Sb galaxy with a bulge/lens plus a low surface brightness disk, viewed at low inclination. The bulge is clearly evident in the profile as is the outer spiral structure. The ellipticity and position angle are not well constrained, but overall the derived parameters agree within their estimated errors.

The final two examples represent worst cases:

AGC 630027 = MCG −2-59-001.—The comparison for this object is shown in Figure 11. This low-inclination SBbc galaxy has open spiral arms that make the ellipse fitting difficult. The tabulated data of MFB, which are not truncated when the

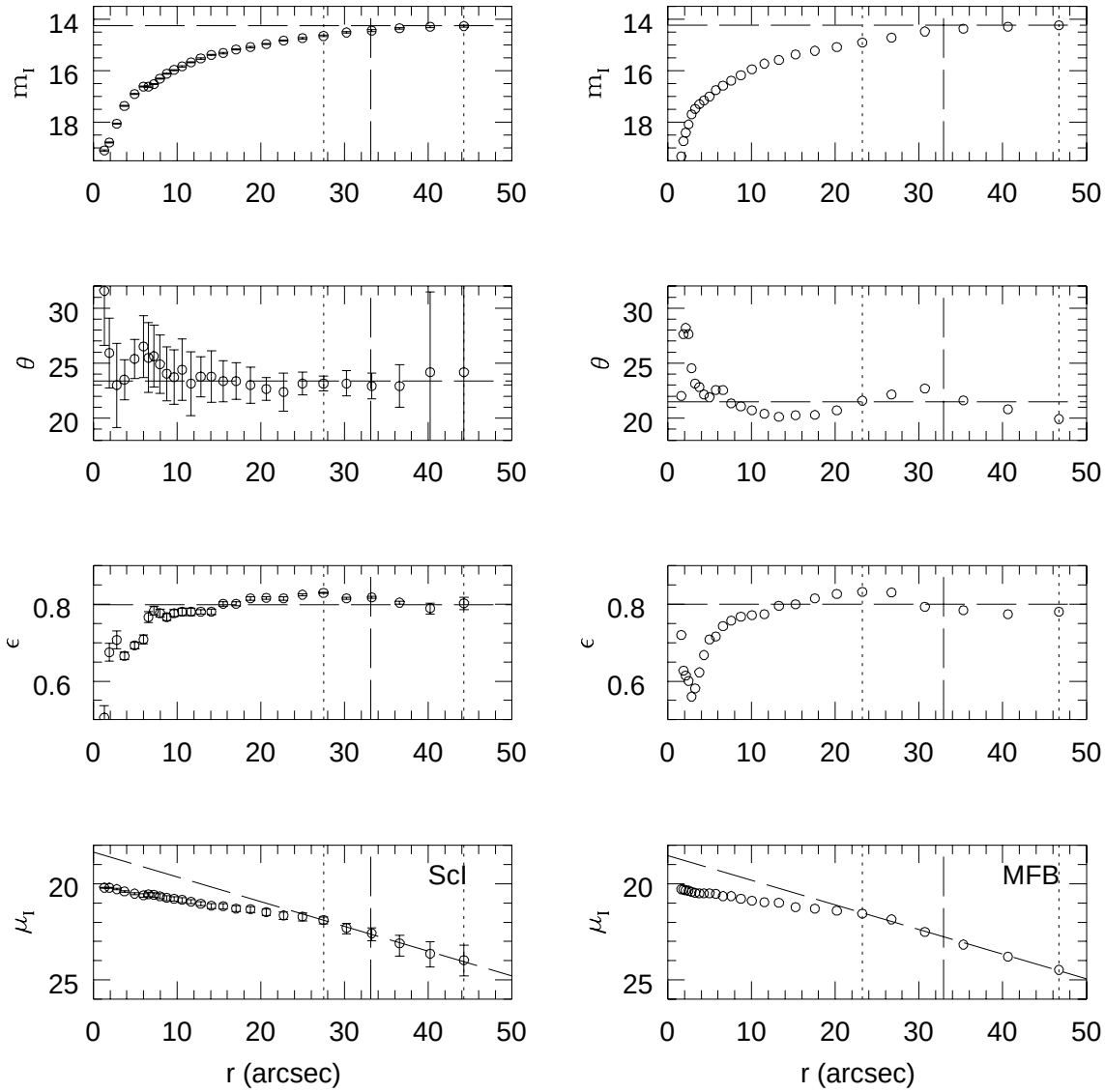

FIG. 7.—Comparison of fitting procedures and results for AGC 430121 = MCG −2-09-021, a highly inclined Sc galaxy. Panels and indicated lines are the same as in Fig. 1.

isophotal intensity reaches some fixed level of the sky noise as in GALPHOT, extend significantly further in radius that the Sc fits, although with roughly constant surface brightness; this extension is clearly the result of the fitting algorithm. The central elongation seen in $\epsilon(r)$ indicates the clear presence of the bar. This galaxy demonstrates the difficulty of fitting the disk because of spiral structure with the result that the magnitudes derived separately are quite discrepant: $\Delta_m = 0.18$.

AGC 31271 = ESO 515G5.—Figure 12 shows the case of ESO 515G5, an Sc galaxy with a lens plus a low surface brightness disk. The Sc image is of relatively low quality with some bleeding from nearby stars, resulting in uncertain determination of the sky noise level. The iteration on the Sc images truncates at a surface magnitude of 22.32 mag arcsec^{-2}. The MFB ellipse fit data extend significantly farther out in the disk. At the same time, the MFB profile appears to level off and then rise at the outer isophotes, perhaps as a result of similar stellar contamination. The ellipticity is not well constrained. The comparison of the magnitudes derived separately using the Sc and MFB image profiles produces one of the most discrepant results, $\Delta_m = 0.24$, apparently because of the uncertainty in fitting the disk and sky.

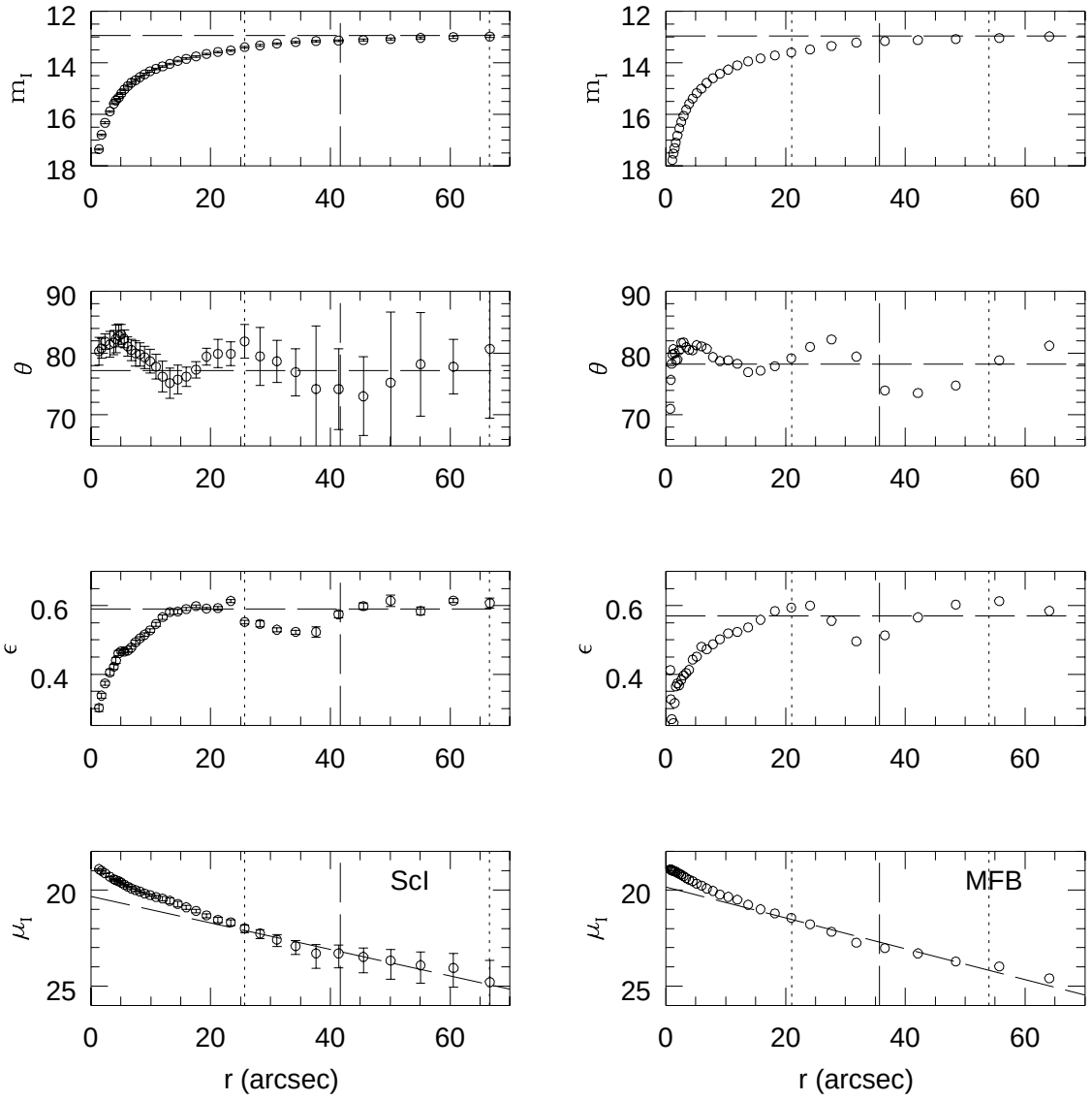

FIG. 8.—Comparison of fitting procedures and results for UGC 139 for both the Sc image (*left*) and the MFB ellipse table (*right*). Panels and indicated lines are the same as in Fig. 1.

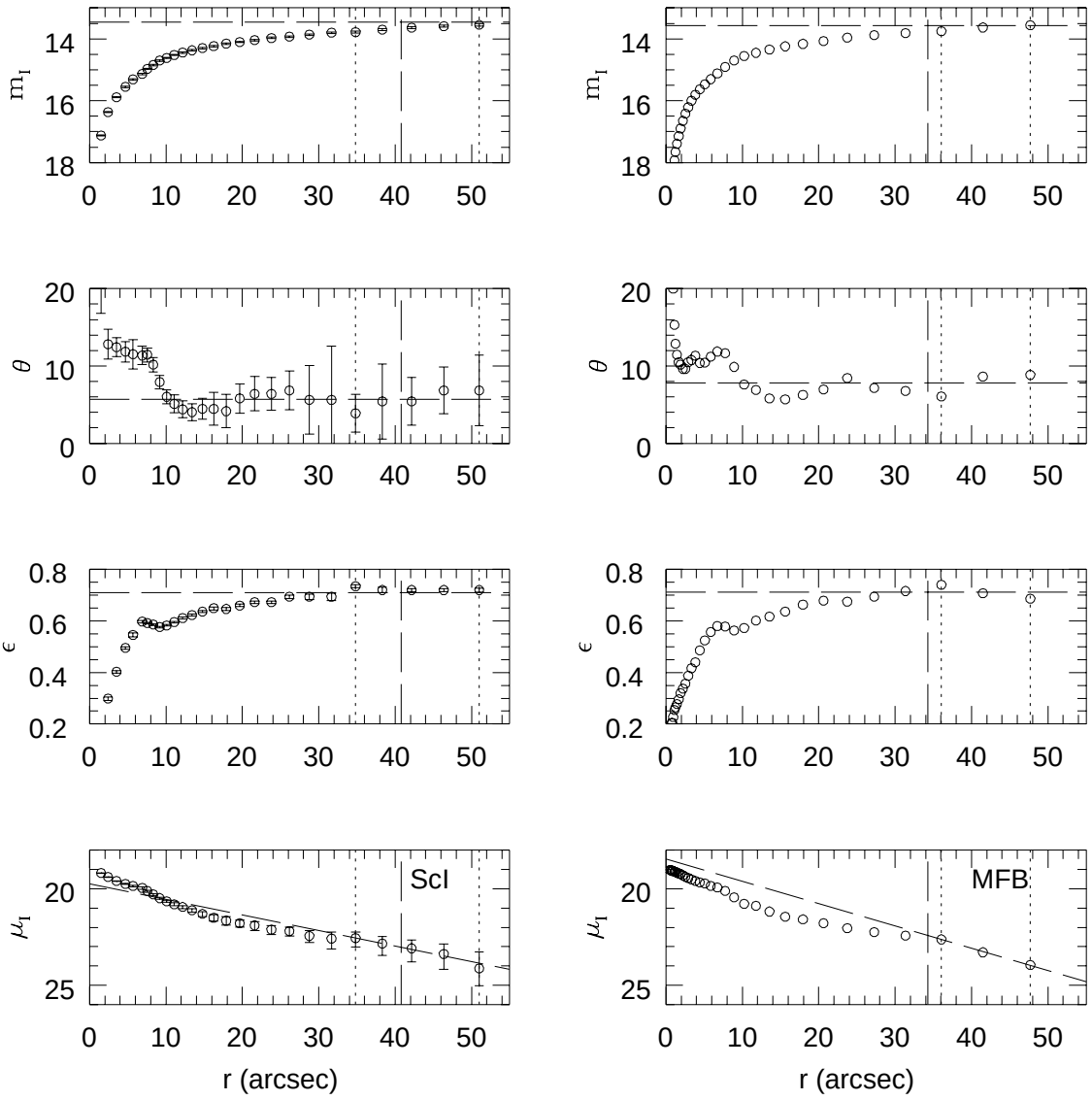

FIG. 9.—Comparison of fitting procedures and results for AGC 400367 = MCG −1-03-005, a moderately inclined Sbc galaxy. Panels and indicated lines are the same as in Fig. 1.

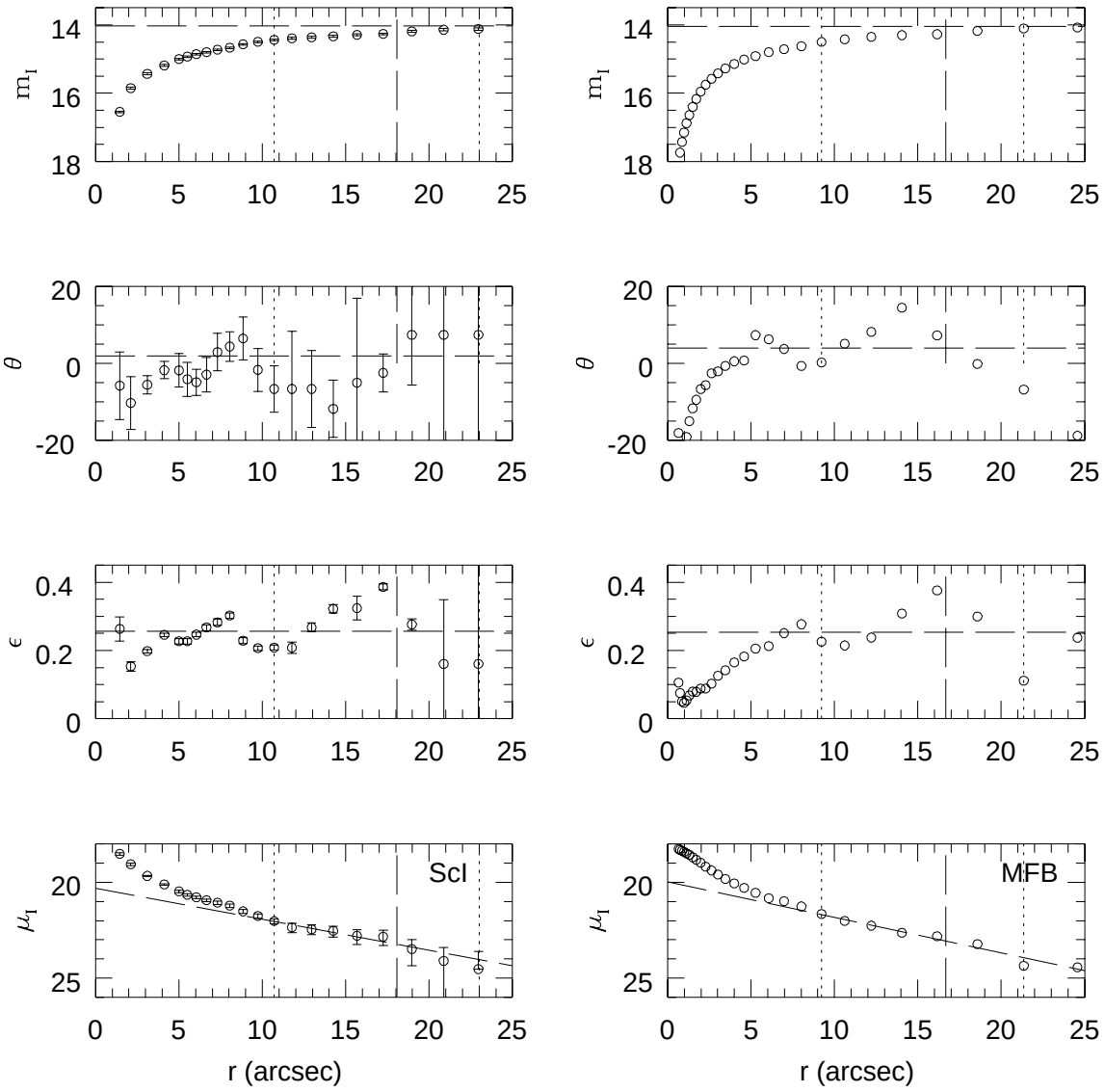

FIG. 10.—Comparison of fitting procedures and results for AGC 260112 = CGCG 108-108, a faint, low-inclination galaxy. Panels and indicated lines are the same as in Fig. 1.

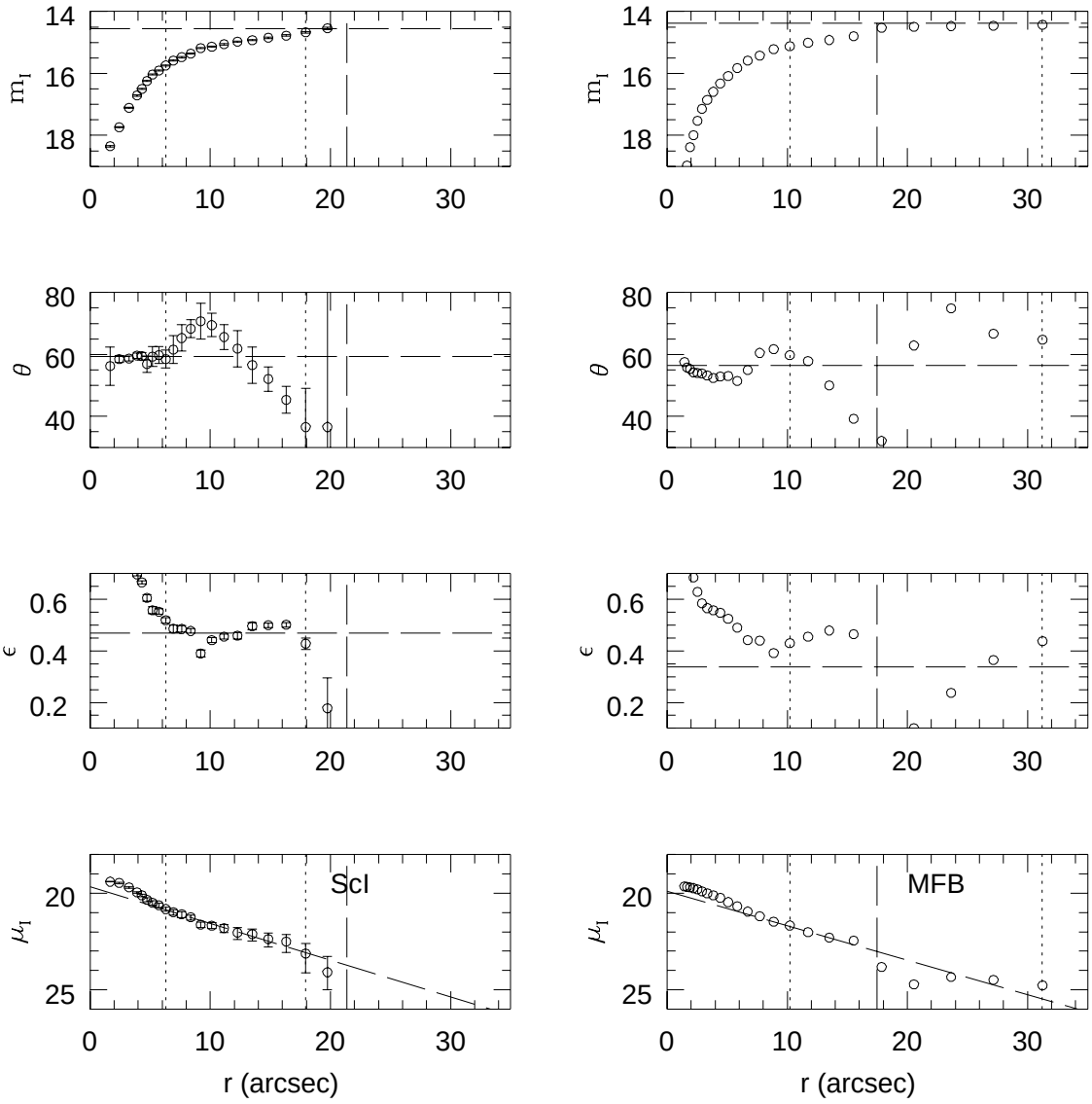

FIG. 11.—Comparison of fitting procedures and results for AGC 630027 = MCG −02-59-001, a barred, low-inclination galaxy, with open spiral arms. Panels and indicated lines are the same as in Fig. 1.

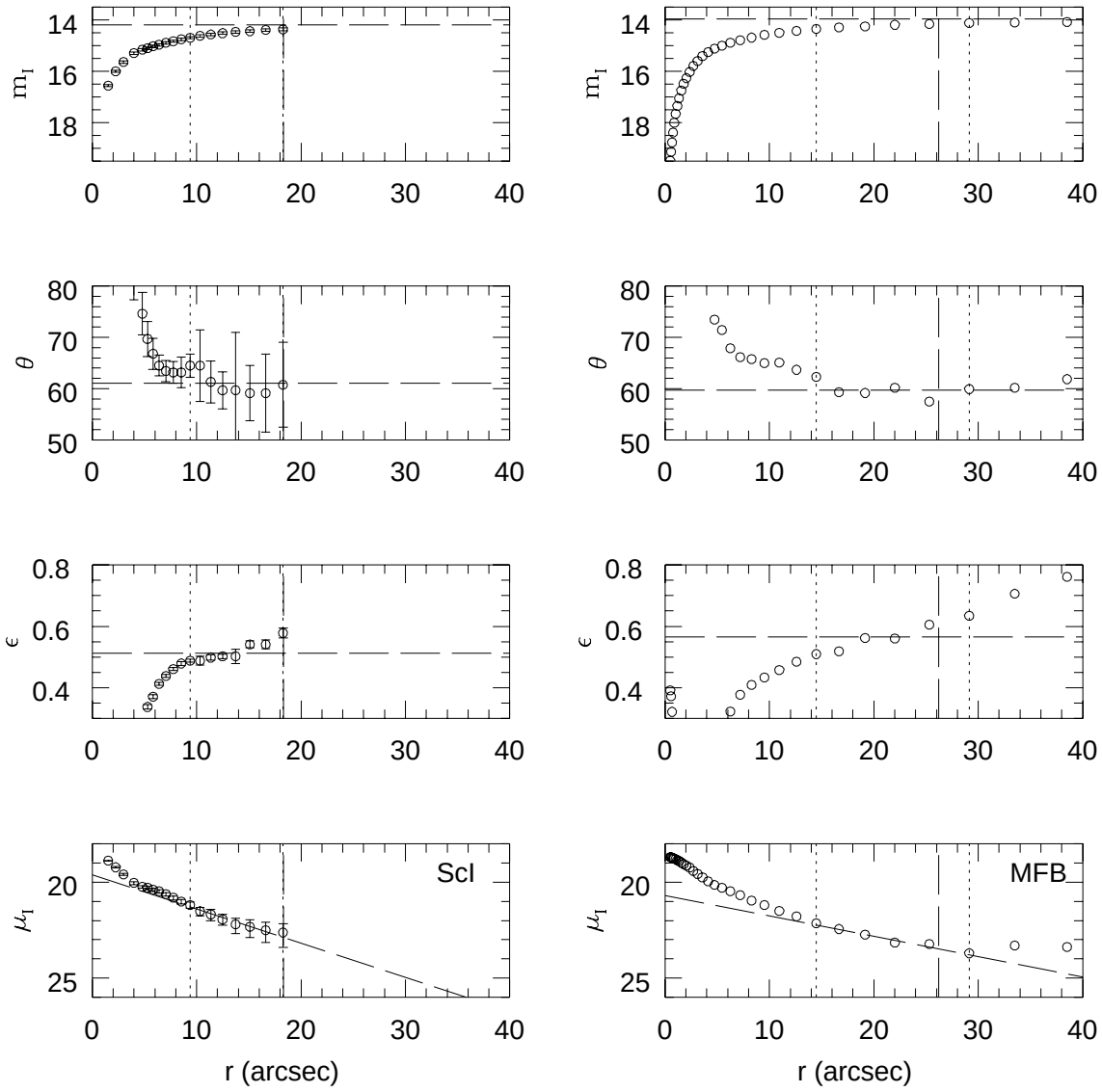

FIG. 12.—Comparison of fitting procedures and results for AGC 31271 = ESO 515-G5, a moderate-inclination galaxy. Panels and indicated lines are the same as in Fig. 1.

REFERENCES

Borgani, S., da Costa, L. N., Freudling, W., Giovanelli, R., Haynes, M. P., Salzer, J. J., & Wegner, G. 1997, ApJ, 482, 121
da Costa, L. N., Freudling, W., Wegner, G., Giovanelli, R., Haynes, M. P., & Salzer, J. J. 1996, ApJ, 464, 99
da Costa, L. N., Nusser, A., Freudling, W., Giovanelli, R., Haynes, M. P., Salzer, J. J., & Wegner, G. 1998, MNRAS, 299, 425
de Jong, R. S. 1996, A&AS, 118, 557
de Vaucouleurs, G., de Vaucouleurs, A., Corwin, H. G., Buta, R. J., Paturel, G., & Fouqué, P. 1991, Third Reference Catalogue of Bright Galaxies (New York: Springer)
Freeman, K. C. 1970, ApJ, 160, 811
Freudling, W. F. 1990, Ph.D. thesis, Cornell Univ.
Freudling, W. F., da Costa, L. N., Wegner, G., Giovanelli, R., Haynes, M. P., & Salzer, J. J. 1995, AJ, 110, 920
Freudling, W. F., Martel, H., & Haynes, M. P. 1991, ApJ, 377, 365
Freudling, W. F., et al. 1998, ApJ, in press
Giovanelli, R., Dale, D. A., Haynes, M. P., Hardy, E., & Campusano, L. 1998a, ApJ, 510, L11
———. 1998b, AJ, submitted
Giovanelli, R., Haynes, M. P., da Costa, L. N., Freudling, W., Salzer, J. J., & Wegner, G. 1997a, ApJ, 477, 1
Giovanelli, R., Haynes, M. P., Herter, T., Vogt, N. P., da Costa, L. N., Freudling, W., Salzer, J. J., & Wegner, G. 1997b, AJ, 113, 22
———. 1997c, AJ, 113, 53
Giovanelli, R., Haynes, M. P., Salzer, J. J., Wegner, G., da Costa, L. N., & Freudling, W. 1994, AJ, 107, 2036 (G94)
———. 1995, AJ, 110, 1059 (G95)
———. 1998c, ApJ, 505, 91
Giovanelli, R., Haynes, M. P., Salzer, J. J., Wegner, G., da Costa, L. N., & Freudling, W. 1998d, AJ, 116, 2632
Giovanelli, R., Haynes, M. P., Wegner, G., da Costa, L. N., Freudling, W., & Salzer, J. J. 1996, ApJ, 464, L99
Haynes, M. P., Giovanelli, R., Chamaraux, P., da Costa, L. N., Freudling, W., Salzer, J. J., & Wegner, G. 1998, AJ, in press
Haynes, M. P., Giovanelli, R., Herter, T., Vogt, N. P., Freudling, W., Maia, M. A., Salzer, J. J., & Wegner, G. 1997, AJ, 113, 1197
Knapen, J. H., & van der Kruit, P. C. 1991, A&A, 57, 61
Landolt, A. U. 1983, AJ, 88, 439
Lauberts, A. 1982, ESO-Uppsala Survey of the ESO(B) Atlas (Garching: ESO)
Mathewson, D. S., & Ford, V. L. 1996, ApJS, 107, 97 (MF96)
Mathewson, D. S., Ford, V. L., & Buchhorn, M. 1992, ApJS, 81, 413
Nilson, P. 1973, Uppsala General Catalogue of Galaxies (Uppsala: Uppsala Astron. Obs.) (UGC)
Paturel, G., Fouqué, P., Buta, R., & Garcia, A. M. 1991, A&AS, 243, 319
Persic, M., Salucci, P., & Stel, F. 1996, MNRAS, 283, 1102
Pierce, M., & Tully, R. B. 1988, ApJ, 330, 579
van der Kruit, P. C. 1979, A&AS, 38, 15
van der Kruit, P. C., & Searle, L. 1981, A&A, 95, 105
Vorontsov-Velyaminov, B. A., & Arhipova, V. P. 1968, Morphological Catalog of Galaxies (Moscow: Moscow State Univ.) (MCG)
Wegner, G., Freudling, W., Haynes, M. P., Giovanelli, R., da Costa, L. N., & Salzer, J. J. 1998, in preparation
Willick, J. 1999, ApJ, in press
Zwicky, F., et al. 1961–1968, Catalogue of Galaxies and of Clusters of Galaxies (4 vols.; Pasadena: Caltech)